

How Tribo-Oxidation Alters the Tribological Properties of Copper and Its Oxides

Julia S. Lehmann, Ruth Schwaiger, Monika Rinke, and Christian Greiner*

Tribochemical reactions in many applications determine the performance and lifetime of individual parts or entire engineering systems. The underlying processes are however not yet fully understood. Here, the tribological properties of copper and its oxides are investigated under mild tribological loading and for dry sliding. The oxides represent the late stages of a copper–sapphire tribo-contact, once the whole copper surface is covered with an oxide. For this purpose, high-purity copper, thermally-oxidized and sintered Cu_2O and CuO samples are tribologically loaded and eventually formed wear particles analyzed. The tribological behavior of the oxides is found to be beneficial for a reduction of the coefficient of friction (COF), mainly due to an increase in hardness. The results reveal tribochemical reactions when copper oxides are present, irrespective of whether they form during sliding or are existent from the beginning. Most strikingly, a reduction of copper oxide to metallic copper is observed in X-ray photoelectron spectroscopy measurements. A more accurate understanding of tribo-oxidation will allow for manufacturing well-defined surfaces with enhanced tribological properties. This paves the way for extending the lifetime of contacts evincing tribo-oxidation.


with a temperature increase in the contact, resulting in oxide formation.^[13,14] Normal and shear stresses are capable to accelerate the rates of chemical reactions and sometimes even their path and with that influence tribo-oxide-formation, friction, and occurring wear mechanisms.^[1,10,15–18] Here, the rate of oxidation is accelerated by orders of magnitude through tribological loading in comparison with native oxidation.^[19] The influence of the formed oxides on the friction and wear response is quite different, depending on the generated oxides: harder and stiffer layers can lead to an increase in wear as well as higher friction.^[20] By contrast, a mechanically softer layer might deform plastically, eventually leading to less wear.^[21,22] In addition, such softer layers can dissipate some of the sliding energy by their growth. Formed oxide films can reduce friction and wear by preventing metal–metal contact,^[23,24] known as mild oxidational wear.^[25] As sliding progresses, a wide and complex range of possible processes can occur: protective “glaze-layers” may form,^[26] wear particles can cause abrasive wear of the metal surfaces,^[27,28] generated oxide films can be removed through tribological loading, and freshly exposed clean metal can be (re)oxidized.^[29] Against the background of these manifold observations of tribo-oxidation, we embark on a systematic investigation with a tribological model setup. Copper was chosen as sample material since it serves as a model system to understand the formation of metal oxides in general.^[30] For native oxidation, copper was found to readily oxidize in two main common forms of oxides: cubic, purple Cu_2O , and monoclinic, black CuO .^[30] To this day, native oxidation of copper is being extensively investigated.^[30] Valladares et al. described a possible oxidation mechanism of a copper surface in an atmosphere with constant oxygen partial pressure:^[31] oxygen is chemically

1. Introduction

Surfaces sliding relative to each other often exhibit chemical reactions between the sliding partners or the partners and the surrounding medium.^[1–3] These chemical reactions impact the tribological properties of a system, resulting in reaction products with different chemical compositions and mechanical properties.^[4] In technical applications, such changes can lead to reduced usability or ultimately to component failure. There have been numerous studies investigating possible tribochemical reactions and the generation of tribo-layers as well as their influence on friction and wear in both lubricated and dry experiments.^[5–8] Among the various reaction products, oxides are recurrently formed.^[1,9–12] Along with the relative motion, the loading is often associated

with a temperature increase in the contact, resulting in oxide formation.^[13,14] Normal and shear stresses are capable to accelerate the rates of chemical reactions and sometimes even their path and with that influence tribo-oxide-formation, friction, and occurring wear mechanisms.^[1,10,15–18] Here, the rate of oxidation is accelerated by orders of magnitude through tribological loading in comparison with native oxidation.^[19] The influence of the formed oxides on the friction and wear response is quite different, depending on the generated oxides: harder and stiffer layers can lead to an increase in wear as well as higher friction.^[20] By contrast, a mechanically softer layer might deform plastically, eventually leading to less wear.^[21,22] In addition, such softer layers can dissipate some of the sliding energy by their growth. Formed oxide films can reduce friction and wear by preventing metal–metal contact,^[23,24] known as mild oxidational wear.^[25] As sliding progresses, a wide and complex range of possible processes can occur: protective “glaze-layers” may form,^[26] wear particles can cause abrasive wear of the metal surfaces,^[27,28] generated oxide films can be removed through tribological loading, and freshly exposed clean metal can be (re)oxidized.^[29] Against the background of these manifold observations of tribo-oxidation, we embark on a systematic investigation with a tribological model setup. Copper was chosen as sample material since it serves as a model system to understand the formation of metal oxides in general.^[30] For native oxidation, copper was found to readily oxidize in two main common forms of oxides: cubic, purple Cu_2O , and monoclinic, black CuO .^[30] To this day, native oxidation of copper is being extensively investigated.^[30] Valladares et al. described a possible oxidation mechanism of a copper surface in an atmosphere with constant oxygen partial pressure:^[31] oxygen is chemically

J. S. Lehmann, Dr. C. Greiner
Institute for Applied Materials (IAM) and MicroTribology Center μTC
Karlsruhe Institute of Technology (KIT)
Karlsruhe 76131, Germany
E-mail: greiner@kit.edu

 The ORCID identification number(s) for the author(s) of this article can be found under <https://doi.org/10.1002/admi.202001673>.

© 2020 The Authors. Advanced Materials Interfaces published by Wiley-VCH GmbH. This is an open access article under the terms of the Creative Commons Attribution-NonCommercial License, which permits use, distribution and reproduction in any medium, provided the original work is properly cited and is not used for commercial purposes.

Prof. R. Schwaiger
Institute of Energy and Climate Research (IEK)
Forschungszentrum Juelich GmbH
Juelich 52425, Germany

Prof. R. Schwaiger
Chair of Energy Engineering Materials
RWTH Aachen University
Aachen 52056, Germany

Dr. M. Rinke
Institute for Applied Materials (IAM)
Karlsruhe Institute of Technology (KIT)
Eggenstein-Leopoldshafen 76344, Germany

DOI: 10.1002/admi.202001673

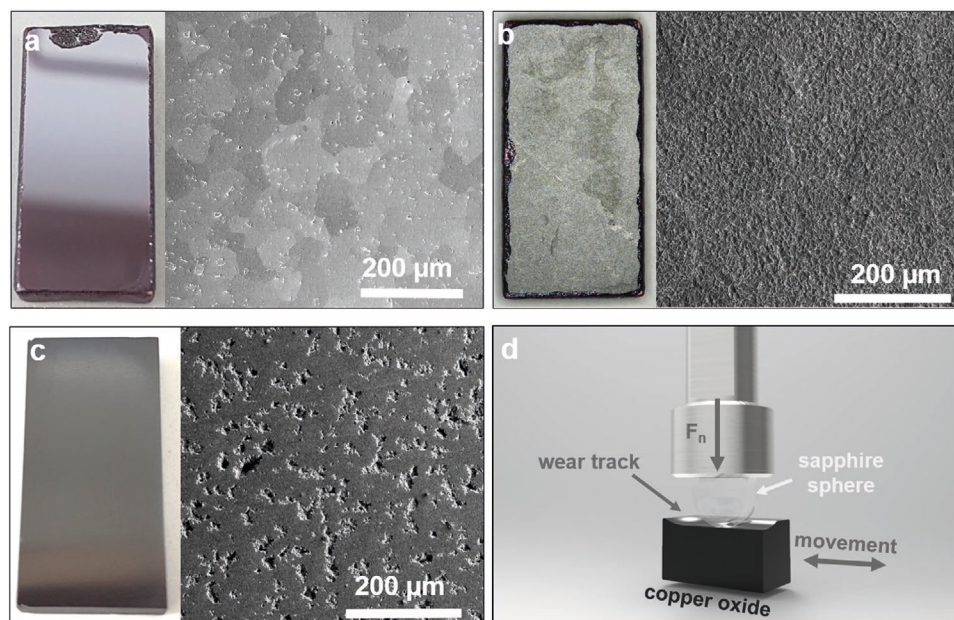


Figure 1. Representative images for the different tested oxides and top-view scanning electron microscopy results of their surfaces: a) thermally oxidized Cu_2O (OPS-polished), b) thermally oxidized CuO (as oxidized), and c) sintered CuO , purchased from Goodfellow (OPS-polished). d) Schematic illustration of the experimental setup with CuO .

absorbed and an oxide layer is formed immediately after the exposure to air. At defects, Cu_2O islands nucleate and expand laterally until they form a Cu_2O film, protecting the surface. Often, a thin CuO layer is formed at the sample surface, followed by a Cu_2O layer underneath.^[32] In turn, a detailed investigation of tribo-oxidation of copper was just recently established. Investigations of Liu et al. yielded proof of Cu_2O island formation under mild tribological loading.^[1] However, the oxides did not grow on, but into the surface. Along with the appearance of the oxides, the coefficient of friction (COF) was found to decrease after 500 sliding cycles. In the light of the multiple and diverse impacts of tribo-oxidation on the tribological performance reported in literature, we ask the following questions: Is this decrease in the COF a result of the oxide formation while sliding? And if so, which oxide characteristics are beneficial for a lower COF? Finally, we will answer the question whether the formed tribo-oxides show the same tribological behavior as the pure oxides. We address these questions by comparing the tribological properties of the pure oxides with the ones of high-purity

copper. The pure oxides represent the late stages of sliding on pure copper, when the whole surface is covered by an oxide. By revealing the intricacies of tribo-oxidation, a future careful tailoring of the materials' surface states might pave the way for enhancing the tribological performance of many technical systems.

2. Results

2.1. Oxide Characterization

A meaningful comparison of the tribological behavior between copper and its oxides requires a careful and thorough sample characterization prior to any tribological experiment. For this purpose, thermally-oxidized Cu_2O and CuO (CuO -TO) and sintered CuO (CuO -S) are fabricated and characterized (**Figure 1**).

The thermally-oxidized samples are analyzed by means of Raman spectroscopy and X-ray diffraction (XRD) (**Figure 2**). A

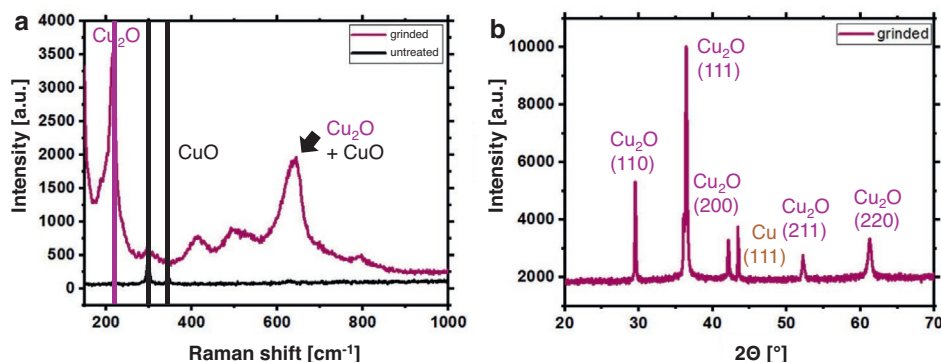


Figure 2. Characterization of the constituents of thermally-oxidized high-purity copper samples. a) Raman spectroscopy of the untreated and grinded sample and b) X-ray diffraction result for the grinded sample.

Table 1. Overview of copper and copper oxides properties: surface roughness, mean grain size, layer thickness, hardness and Young's modulus (both determined by nano-indentation) and chemical composition (determined by EDS).

	Cu-OFHC	Cu ₂ O	CuO-TO	CuO-S
Final surface preparation step	Electro-polished	OPS-polished	As oxidized	OPS-polished
Color	Copper-colored	Purple	Black	Black
S _a [nm]	96 ± 18	24 ± 4	1463 ± 291	90 ± 14
Mean grain size d [μm]	40	70	n/a	n/a
Layer thickness [μm]	n/a	175–190	240–260	n/a
Hardness [GPa] (averaged over indentation depth [nm])	n/a	2.94 ± 0.02 (1800–2000)	2.28 ± 0.7 (2500–2900)	2.51 ± 0.42 (1600–1800)
Young's modulus [GPa]	117	41 ± 0.2	37.5 ± 5.9	70.6 ± 5.0
Chemical composition [at%]	Cu	99 ± 1	70 ± 1	48 ± 1
	O	2 ± 1	30 ± 1	52 ± 1

two layer structure is observed: CuO on top of Cu₂O. Figure 2a displays characteristic Raman–CuO peaks for the untreated sample, while the grinded sample also exhibits Cu₂O peaks. X-ray spectroscopy was deployed to further investigate the grinded sample (Figure 2b).

Surface topography, color, roughness, layer thickness, hardness, Young's modulus, and chemical composition vary between the oxides (Table 1).

Cu₂O is purple, whereas CuO appears black. Both, Cu₂O and the CuO–S sample exhibit pores. Individual oxide islands are visible on the CuO–TO sample. Surface roughness of the polished samples vary from S_a = 25–100 nm, among which the electro-polished Cu–OFHC samples show the highest value with 100 nm. A 15-times higher roughness is observed for the CuO–TO sample (S_a ≈ 1500 nm). The average grain size of 70 μm for the Cu₂O sample is 30 μm larger than the average grain size for the Cu–OFHC copper (≈40 μm). The other grain sizes could not be measured due to the samples' surface topography. A layer thickness of 240–260 μm is obtained after 1 h in air at 1000 °C for CuO–TO; thickness was measured in transverse micro sections. Raman-spectra reveal that this layer comprises both oxides (Cu₂O and CuO, Figure 2a). After grinding the topmost CuO layer away, the underlying layer thickness of the Cu₂O sample is 175–190 μm. Nano-indentation measurement results are summarized in Figure S1, Supporting Information. CuO–TO's hardness is the lowest (2.28 ± 0.7 GPa), whereas the highest was found for Cu₂O (2.94 ± 0.02 GPa). With 2.51 ± 0.42 GPa, the CuO–S sample is located in the middle. The hardness of Cu–OFHC was not measured by nano-indentation and is therefore not given in Table 1. The Young's modulus for CuO–S with 70.6 ± 5.0 GPa, is almost twice as high as the modulus for CuO–TO with 37.5 ± 5.9 GPa. The modulus of Cu₂O lies with 41 ± 0.2 GPa in the middle. Energy-dispersive X-ray spectroscopy (EDS) results reveal the chemical composition of the samples before tribological loading (Table 1). The high-purity copper has up to 2 at% of oxygen, Cu₂O around 30 at%, and the CuO samples ≈50 at%.

2.2. Tribological Properties, Wear Particle Formation, and Characterization

With the tribological setup schematically displayed in Figure 1d, the COF was determined and is presented in Figure 3a.

Each curve represents the mean value of two experiments. Cu–OFHC demonstrates the highest COF within the first 4000 cycles. In contrast, Cu₂O exhibits the lowest COF for all oxides (mean value for steady state COF ≈ 0.18). CuO–S and CuO–TO show a steady COF after 500 cycles. CuO–S has almost a factor of two smaller COF than the thermally-oxidized sample. Figure 3b displays the wear track profiles after 5000 cycles and Table 2 summarizes the measured wear track widths and depths. We make use of the commonly used assumption that the depth of the wear track is a measure for the wear volume.^[33] While pure copper exhibits the formation of a wear track with a depth of ≈2 μm after 5000 and 10 000 cycles, the oxides evince either no wear track, or patches, or holes (Figure 3). Increasing sliding cycles result in a broadening of the wear track for Cu–OFHC (5000 vs 10000 cycles) from ≈175 to 270 μm. The profile along the wear track of the CuO–TO indicates a wavy behavior (Figure 3c, the wear track is marked by an arrow).

Light microscopy images of the spheres and plates after 5000 cycles are presented in Figure 4. Scanning electron microscopy images of the wear tracks on copper and its oxides after 5000 cycles are summarized in Figure S2, Supporting Information. Cu–OFHC exhibits a purplish coloring of the wear track and small particles on the sapphire sphere (Figure 4a,b). EDS measurements inside the wear track show up to 22 at% of oxygen (Table 3). Up to 3 at% of aluminum is present on the high-purity copper plate after 10000 cycles.

The wear tracks and spheres of the copper oxides display the formation of yellowish wear particles (Figure 4c–h). These particles are visible after sliding on all the tested oxides and accumulate primarily at the ends of the wear tracks. Light scratches are present inside the wear track of Cu₂O, whereas the CuO–TO sample exhibits an unsteady wear track, with some parts displaying the purplish color of the underlying Cu₂O layer. For pure copper run for 10000 cycles, the formation of yellowish wear particles is visible (Figure 5). The COF decreases to 0.37 after 5000 sliding cycles.

Table 3 and Figure 6 show the results of the chemical analysis of the wear tracks and particles. For the sintered CuO, EDS measurements reveal up to 2 at% of aluminum after 5000 cycles inside the wear track (Tables 3 and 4), whereas the other oxides show no aluminum. For Cu₂O, the concentration after sliding was the same as prior to sliding. However,

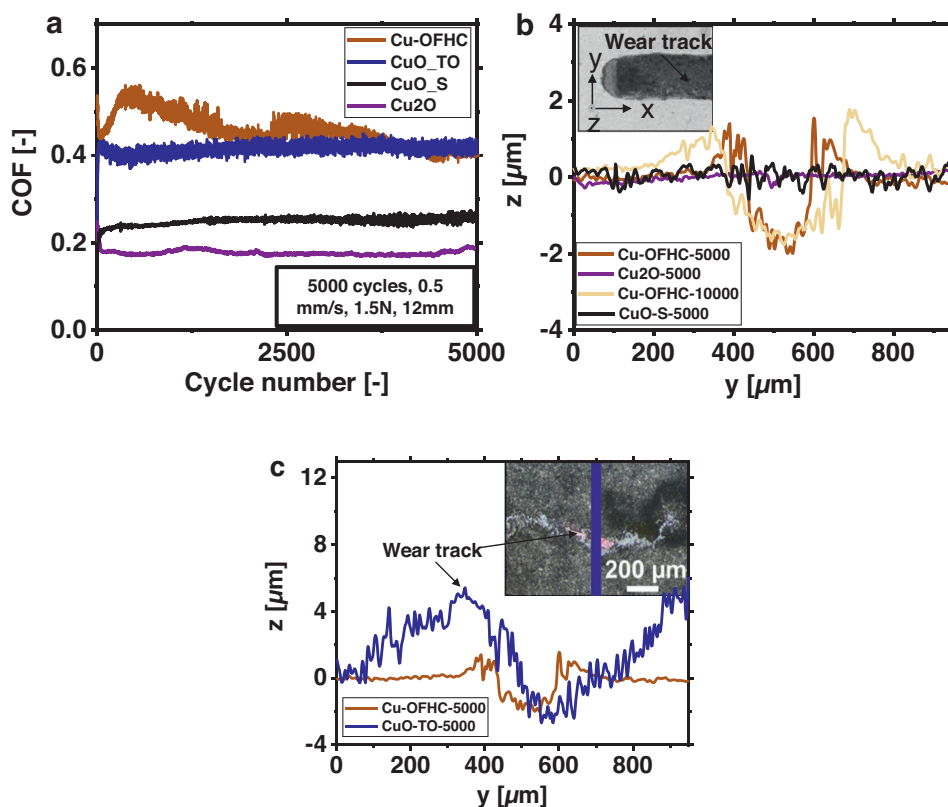


Figure 3. Coefficient of friction (COF) and wear track profiles. a) Mean values of two experiments for the coefficient of friction (COF) of thermally oxidized Cu_2O , CuO (CuO-TO), sintered CuO (CuO-S), and high-purity copper (Cu-OFHC). b) Depth profiles measured in the middle of each wear track and the respective coordinate system shown in a confocal microscope image. c) Depth profiles for CuO-TO in comparison with Cu-OFHC . The small confocal microscope image represents the wear track of the CuO-TO sample, and the position profile (blue line).

for CuO-TO and CuO-S , the copper concentration increased (65 ± 1 and 57 ± 9 at%).

X-ray photoelectron spectroscopy (XPS) measurements of the wear particles found on the sapphire sphere in contact with CuO-S were performed (Figure 6). Two different positions were analyzed: (1) inside the contact area and (2,3) two spots on the formed wear particles (Figure 6a). Depth profiles up to 100 nm depth inside the contact area (1) and on a wear particle (2) are displayed in Figure 6c,d. Aluminum, oxygen, copper, and carbon are detected. After approximately 5 nm, the carbon concentration decreases below 1 at% (1) inside the wear track and (2) below 10 at% inside the wear particles. For (1), the concentration of aluminum and oxygen stays almost constant up to 100 nm, representing Al_2O_3 (see also Figure 6i). Within the wear particles (2) up to 10 at% of copper is measured, starting at ≈ 5 nm below the surface up to a depth of 100 nm. The oxygen concentration increases slightly from 28 at% at the surface to ≈ 33 at% in the

bulk, whereas carbon concentration decreases successively from the surface to the bulk (from ≈ 40 at% at the surface to ≈ 5 at% at 100 nm). At the wear particles surface, CuO is observed (Figure 6e), accompanied by aluminum hydroxides, carbon monoxides, and hydrocarbons (Figure 6f,g). In 100 nm depth, metallic copper inside the wear particles is found (Figure 6j).

In two experiments for Cu_2O and CuO-S , a strong increase in the COF is detected with higher sliding cycles (from 0.2 to 0.6 for Cu_2O and from 0.22 to 0.45 for CuO-S , Figure 7a). At the same time, an increased yellow wear particle formation is observed both on sphere and plate (Figure 7b–e). Figure S3, Supporting Information, shows a top- and cross-sectional view on a pore, filled with wear particles of the CuO-S experiment in Figure 7d. Scanning electron microscopy images of the wear tracks the plates in Figure 7 are summarized in Figure S2, Supporting Information.

Table 2. Wear track widths and depths measured in confocal microscopy images in the middle of the wear track.

	Cu-OFHC 5000 cycles	Cu-OFHC 10000 cycles	Cu_2O	CuO-TO
Wear track width [μm]	268 ± 5	367 ± 6	168 ± 39	232 ± 131
Wear track depth [μm]	1.9 ± 0.1	1.8 ± 0.1	n/a	n/a

3. Discussion

3.1. Material Characteristics Influencing Friction and Wear Behavior

We first pose the question which material characteristics influence the tribological properties and in which way. The results are discussed considering the different oxide surface

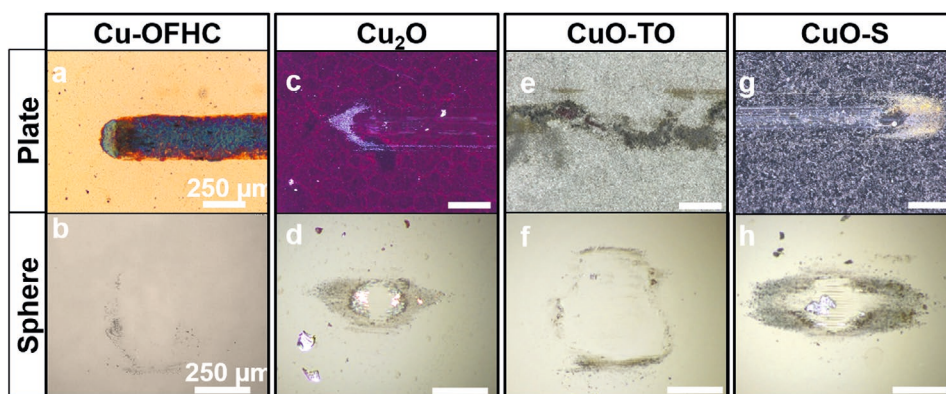


Figure 4. Light microscopy images of the plates and spheres after 5000 sliding cycles. a,b) Cu–OFHC, c,d) Cu₂O, e,f) CuO–TO, and g,h) CuO–S. The scale bar is 250 μm.

topographies. Comparing the surface roughness and hardness of the tested samples hints into the following direction: all oxides exhibit a lower COF than the high-purity copper (Figure 3a). One might argue that the COF depends on the sample's different surface roughness. Literature suggests an influence of roughness on the COF, particularly a decrease in COF with rougher surfaces for dry sliding.^[34,35] For example, Sedlaček et al. found a lower COF for high surface roughness for pin-on-disc tests with 100Cr6 steel discs and an Al₂O₃ ball.^[34] Additionally, the sliding distance to steady-state friction conditions tended to become longer.^[34] Under fretting conditions, Kubiak et al. reported a strong influence of initial surface roughness on the friction and wear processes for a steel (AISI 1035) and a titanium alloy (Ti-6Al-4V):^[35] for rough surfaces, a lower COF and higher wear rate were found. In our experiments, the surface topography varied for the different oxides (Figure 1 and Table 1). Thermal oxidation generated islands, which coalesced with ongoing oxidation, as often reported in literature.^[31,36] In between these islands, void-like structures are observed (Figure S4, Supporting Information). Such features were also found by Heinemann et al. for copper oxidation.^[37] In addition, different surface roughness was obtained as a result of different preparation methods (Table 1). How does the roughness affect the COF in our experiments? In contrast to previous observations in literature, Figure S5, Supporting Information, reveals that the mean COF for the first 10 cycles does not correlate with the initial surface roughness. The surface roughness values of Cu–OFHC, Cu₂O, and CuO–S are below 150 nm, and should have based on the findings in

Table 3. EDS results for a high-purity copper sample after 10000 sliding cycles, and for Cu₂O, CuO–TO, and CuO–S samples after 5000 cycles in at%.

	Cu–OFHC		Cu ₂ O	CuO–TO		CuO–S	
	Wear track	Wear particles	Wear track	Wear track	Wear track	Hole	Patch
Cu	78 ± 1	77 ± 12	71 ± 1	65 ± 1	57 ± 9	50 ± 2	53 ± 3
O	22 ± 1	21 ± 10	29 ± 1	35 ± 1	43 ± 9	48 ± 1	46 ± 2
Al	–	2 ± 1	–	–	1 ± 1	–	1 ± 1
Si	–	2 ± 2	–	–	–	2 ± 1	–

literature – a lower COF. However, Cu–OFHC shows a higher COF than all oxides (factor ≈1.8–3 higher). One possible explanation for this behavior is a hardness difference, which will be discussed later. Is this observation of the absence of a roughness influence still valid for higher cycle numbers? CuO–TO exhibits an exceptionally high initial roughness ($S_a \approx 1500$ nm) in comparison with the other samples ($S_a < 150$ nm) (Table 1). Indeed, we can speculate this being the reason for the larger COF of CuO–TO in contrast with the other oxides. Interestingly, the COF of CuO–TO is still below the COF of the high-purity copper sample (<4000 cycles, Figure 3a). On the one hand, roughness influences the COF within the same material (CuO–TO vs CuO–S), while on the other hand, the type of material (high-purity copper vs copper oxide) has a more pronounced influence on the COF than the sample roughness (Figure 3a). Therefore, the influence of the different surface morphologies seems not to be the pivotal reason for the lower COF.

A significant number of existing studies in literature associate lower COFs with higher hardness.^[38,39] For this reason, oxide hardness was determined by nano-indentation measurements (Figure S1, Supporting Information). We found a higher hardness for the oxides than for pure copper (hardness of annealed and electro-polished Cu–OFHC: 42 HV0.1). Cu₂O exhibits the highest values among all oxides, possibly explaining the lowest COF (Figure 3a). The wear track depth and width (Figure 3b,c and Table 2) demonstrate the hardness influence in more detail: for Cu₂O and CuO–S both, width and depth of the wear track, are smaller than for the pure copper. Thus, the sapphire sphere mainly slides on the oxide surfaces without indenting into the material, as is the case for the softer copper (Figure 3b). Ploughing through copper requires more energy, resulting in a higher COF. The size of the contact area on the spheres supports this finding (Figure 4b,d,f,h): Cu₂O and CuO–S exhibit a smaller contact area than Cu–OFHC. An exception from this trend is the CuO–TO sample where the high roughness of the plate leads to a larger contact area and the sphere is mainly sliding on these individual islands (Figure 3c, Figure 4e,f, and Table 2). This sample is composed of a thin CuO layer on top of Cu₂O (Raman spectroscopy and XRD-analysis, Figure 2).^[40–44] Such a sequence of layers and layer thicknesses are in agreement with literature (Table 1).^[30,45] A removal of the top CuO

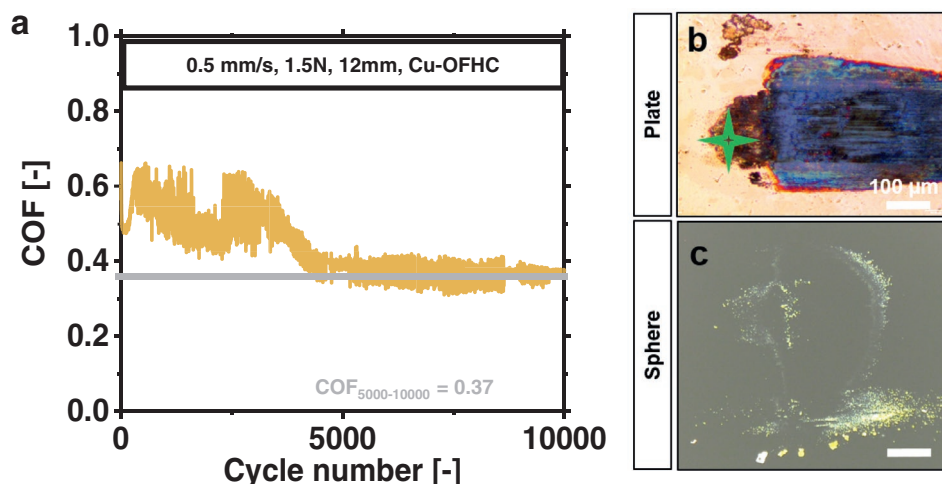


Figure 5. Cu—OFHC sliding against sapphire for 10000 cycles. a) Coefficient of friction, b,c) light microscopy images of copper plate and sapphire sphere, respectively. The scale bar is 100 μm . Coloring of the wear track and formation of wear particles on the sphere and plate. The star in (b) marks the position for the EDS measurements listed in Table 3.

layer thorough the sliding sphere is observed, ultimately resulting in a patchy wear track (Figure 4). EDS measurements corroborate this finding: inside the wear track, a composition close to Cu_2O is detected (Table 3). The tribological properties measured are superimposed from both oxides, at least for the late stages of sliding. We do not know the exact layer thickness of CuO on-top of Cu_2O , so no comments on how long the CuO layer sustains sliding can be made. For Cu_2O however, the oxide thickness is sufficient for a pure oxide contact: the sphere did not break through the Cu_2O layer (180–260 μm). In addition to hardness, shear strength is an important factor influencing wear mechanisms and friction.^[46] The interface adhesion strength is expected to be different between sapphire/copper and sapphire/copper oxide. Metallic oxides usually exhibit a higher interfacial shear strength.^[47] Bowden and Tabor pointed out that while moving two bodies tangentially, the friction force is a function of the real contact area and the junction's shear strength.^[46,48] Depending on the hardness of the body, the contact area and shear strength deviate: the contact of a hard body sliding against a soft body shows a large contact area and low shear strength (copper vs sapphire) while the contact of two hard bodies exhibits a small contact area but large shear strengths (copper oxides vs sapphire).^[46,48] Copper has a relatively low shear strength around 1.5 GPa, resulting in a higher degree of plowing and more energy is dissipated while sliding (Figure 3a,b).^[48] Mishra et al. reported a change in wear behavior from plowing to wedging (deformed substrate material stacked in front of the sliding asperity and possibly material transfer, Figure 4d,g) with increased shear strength.^[47,49] Hence, oxides with higher shear strength are expected to show less or no plowing. In addition, a soft interfacial medium or film between the two contacting bodies may lead to a small contact area and small shear strengths within the film, ultimately resulting in a low coefficient of friction. Section 3.2 discusses the last scenario. In summary, increased hardness and different size of contact area and shear strength of the oxides in comparison to pure copper is suspected to be the primary reason for the lower COF and different observed wear behavior. Along

with the hardness, the different Young's modulus might further contribute to the lower friction forces observed.^[4,15,46]

3.2. Wear Particle Formation, Characterization, and Their Influences on the Tribological Properties

Earlier investigations with copper and sapphire showed no wear particle formation up to 1000 cycles.^[1] Surprisingly, all samples in our experiments show the formation of yellowish wear particles on the sphere as well as on the plate (Figures 4 and 5). We applied XPS and EDS to analyze these wear particles (Table 3 and Figure 6). Exemplarily the XPS results for a sphere after 5000 cycles in contact with CuO—S (Figure 4h) are presented in Figure 6. This data gives evidence for the presence of copper (up to 10 at%) on the sphere and for aluminum on the plate (up to 2 at%) (Table 3 and Figure 6). In combination with the yellow color, these findings bear witness on reactions between the tribo-partners while sliding. Silicon may come from the sample preparation. Interestingly, copper is solely found within the wear particles on the sphere, and not in the contact area (Figure 6c,h). The mapping in Figure 6h displays the distribution of copper and carbon on the sphere. Here, carbon may come from the environment and physically adsorb at the sample surface. The contact area on the sphere only consists of Al_2O_3 (Figure 6c,i). Since both elements, copper and aluminum, are found in the wear particles, it is very likely that the reaction between CuO and Al_2O_3 takes place inside the contact area. Reaction products are then removed from the contact area through sliding. A closer look at the wear particles reveals an astonishing finding: they are comprised of CuO at the particle surface and metallic copper inside (Figure 6g,i). Sliding provides enough energy to reduce copper oxide to metallic copper. It is Al_2O_3 's high enthalpy of formation which may lead to this reduction (formation enthalpy: Al_2O_3 ($-1675,7 \text{ kJ mol}^{-1}$), Cu_2O (-169 kJ mol^{-1}) and CuO (-157 kJ mol^{-1}). As a result of this reduction, a CuAl alloy forms, exhibiting its characteristic golden-yellowish color.^[50] This alloy therefore most

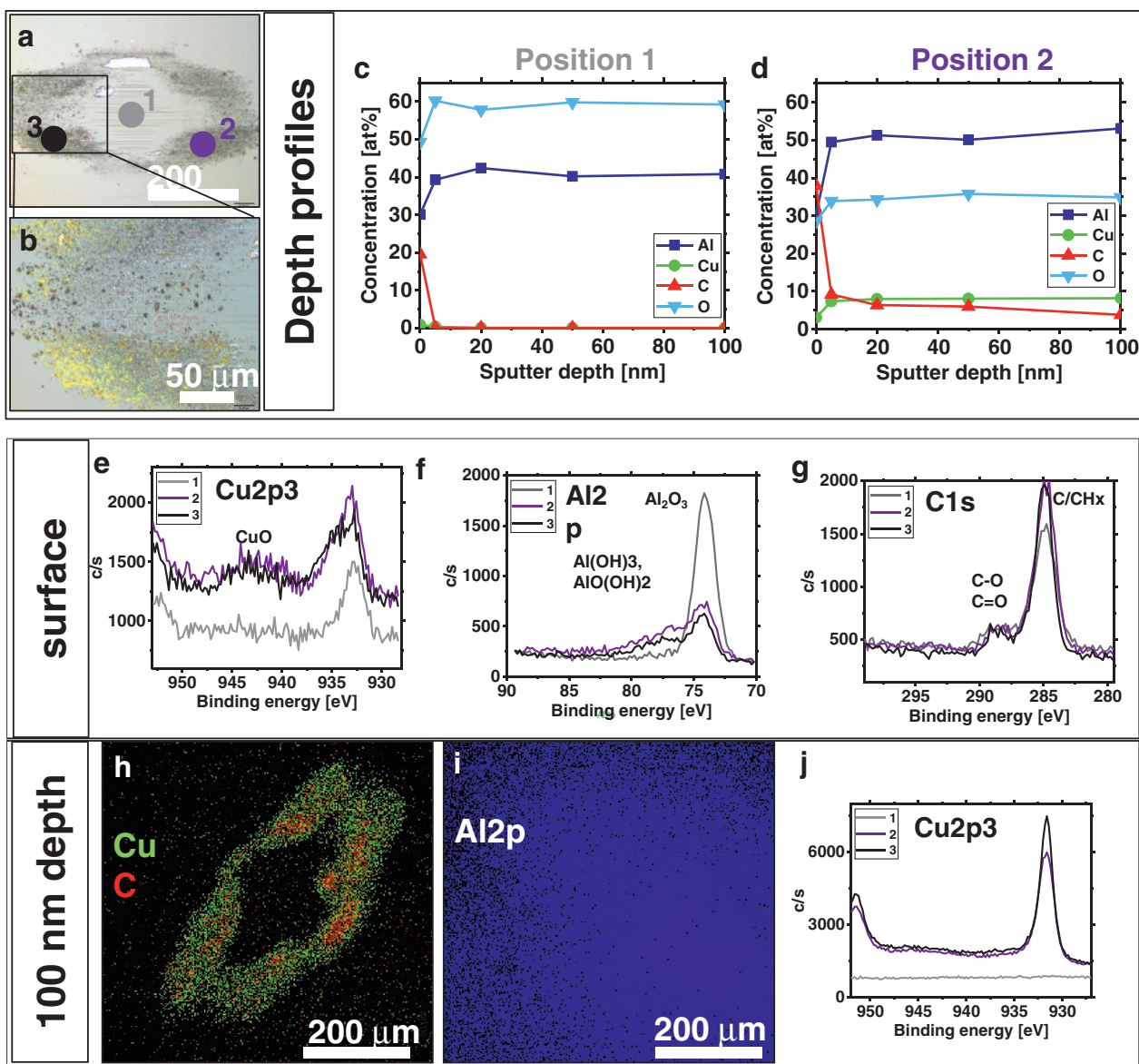


Figure 6. Wear particle analysis of a sapphire sphere after 5000 cycles of sliding against CuO–S. a,b) Light microscopy images of the sapphire sphere and wear particles. c–j) X-ray photoelectron spectroscopy analysis of the sapphire sphere: c,d) depth profiles for 0–100 nm depth. e–g) Surface spectra for copper, aluminum, and carbon. h,i) Copper, carbon, and aluminum mapping of the sphere in 100 nm depth. j) Copper spectrum in 100 nm depth. The overview spectra were measured with a pass energy of 187 eV, and the element spectra with 23 eV. The mapping was performed at 15 kV, 2.5 W, with a beam diameter of $\approx 15 \mu\text{m}$ and a pass energy of 187 eV.

likely is present in the wear particles, alongside with Al_2O_3 and surrounded by an oxidized outer layer of Al_2O_3 and CuO (Figure 6d–g,j). Cu–Al alloys are known for their excellent wear

Table 4. EDS results for samples showing increased wear particle formation: CuO–S and Cu_2O after 5000 sliding cycles in [at%].

	CuO–S		Cu_2O	
	Wear particle	Wear track	Dark areas	Wear particle
Cu	31 ± 1	67 ± 5	61 ± 1	69 ± 1
O	54 ± 2	33 ± 5	39 ± 1	28 ± 1
Al	16 ± 3	–	–	3 ± 1

resistance in comparison with other copper alloys.^[51] From Section 3.1 one might expect that an interfacial film comprised of a layer with a lower shear strength than the contacting bodies lowers the coefficient of friction. Since the amount of such wear particles is not sufficient to form a uniform, closed layer, these properties most likely do not contribute in a considerable way to the overall tribological performance. Indeed, we observe that wear particle formation did not alter the COF (Figure 3a). Only the CuO–S experiments show a slightly noisier friction signal for <3000 cycles which might correlate with wear particle formation.

In the Cu_2O experiment, another type of wear particle formation is observed: a $\approx 100 \times 140 \mu\text{m}$ rectangular wear particle is

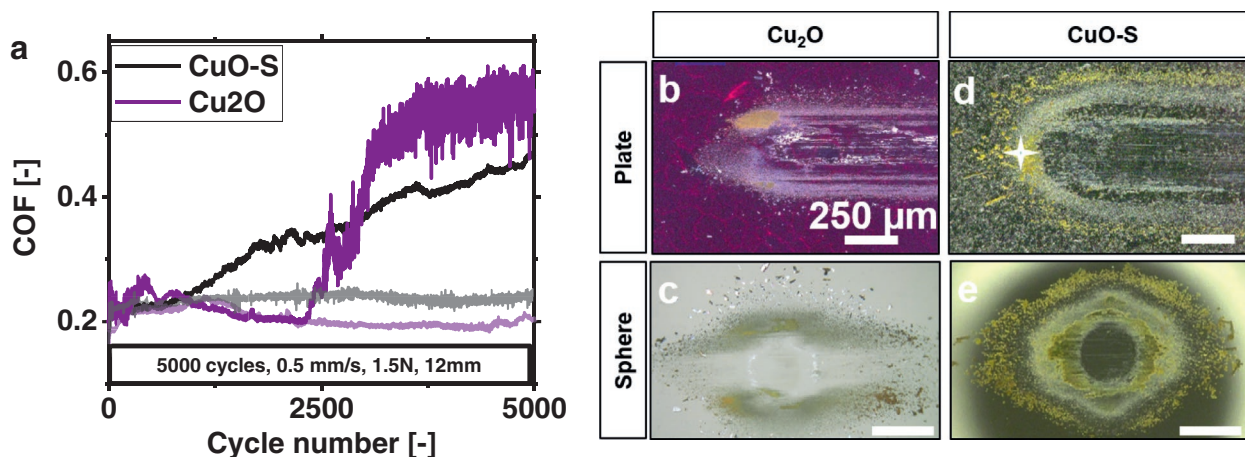


Figure 7. Two experiments with increased wear particle formation: Cu₂O and CuO–S after 5000 cycles. a) COF for CuO–S and Cu₂O with increasing cycle number in comparison (full-colored lines) with two samples exhibiting a steady state COF (half-transparent lines). Light microscopy images of the b,c) Cu₂O plate and sphere and d,e) CuO–S plate and sphere. The scale bar is 250 μm.

visible on plate and sphere (Figure S6, Supporting Information) and almost no wear track formation is found. This particle indicates that the sphere successively removed thin layers of Cu₂O and compacted this layer to a bigger particle. The formed wear particle exhibits stronger atomic bonding than with the plate or sphere. However, this particle does not show a yellowish color, but almost the same color as the Cu₂O. EDS measurements of the particle show the same chemical composition as within the wear track (Table 3). Such behavior may be associated with a higher ductility of Cu₂O than for CuO.^[52] The COF is not altered by this process and almost constant for >20 cycles.

Traces of an adhesive wear mechanism for CuO–S are visible in ex situ light microscopy images (Figure S7, Supporting Information). This material displays areas where pieces broke out of the wear track. Ultimately, this results in holes with a depth of up to 6 μm. Some patches with a height of approximately 1 μm are present. These patches stay attached to the sphere or reattach to the oxide: by closely looking at the sphere in Figure 4h, two large patches at its tip are visible. EDS measurements of the plate identified these as slightly copper rich (53 ± 3 at%), whereas the holes are mainly comprised of CuO with up to 3 at% of aluminum. The wear track next to the patches and holes contains up to 57 ± 9 at% of copper and up to 2 at% of aluminum. Possibly, these areas are compacted wear particles and therefore may have the same characteristics (Figure 7). The patches could be a result of adhesive forces in the contact with the sphere. Due to the porosity of this sample, chemical bonding might be larger among the reaction products from sliding than within the material itself.

For all oxides, we find that wear particle formation did not alter the COF up to 5000 sliding cycles (Figure 3a). However, two among the performed experiments showed a different behavior: a strong increase in both, wear particle formation and COF (Cu₂O and CuO–S, Figure 7). For Cu₂O, the COF increases by about factor of three (from 0.2 to 0.6) during the 5000 cycles. First, the COF is stable around 0.2 and then increases within ≈1500 cycles to 0.6. For CuO–S, the increase in COF is almost linear with the cycle number (from 0.22 to

0.45). We relate the increased COF to the onset of increased wear particle formation. We can only speculate about why this happens.

The steady increase in COF for CuO–S might have two reasons: aluminum bronze formation along with increased adhesion and an increase in the contact area through compacted wear particles. A concentration of up to 18 at% of aluminum is present on the plate after 5000 cycles on CuO–S, supporting the theory of aluminum bronze formation. In the Al–Cu phase diagram, the α-solid solution is prevailing up to 18 at% of aluminum and no intermetallic phase is present. In previous studies on the tribological behavior of aluminum bronzes, an increase in the COF with higher aluminum content was reported.^[5] This was explained by stronger adhesion and metallic transfer.^[5] Poggie et al. tested aluminum bronzes with different aluminum content against an Al₂O₃ cylinder in unlubricated reciprocating sliding.^[53] For 10 000 sliding cycles (=508 m) and an aluminum content of 6 wt%, they observed a final COF of 0.91. In comparison, we find a COF of 0.45 (Figure 7a) for the sintered CuO after 5000 cycles (=120 m). One could thus speculate that the aluminum content increases with the sliding cycles for the sintered sample and, after a certain point, also for Cu₂O. This is supported by the experiments without increased wear particle formation, which all exhibit aluminum contents below 3 at% (Table 3). An increased wear particle formation may be associated with a “critical” aluminum concentration within the Cu–Al alloy. Another finding in literature is that aluminum segregates to the surface and forms aluminum oxide in tribological experiments with Cu–Al alloys.^[5,54] This would result in a self-paired contact and a further increase in adhesive wear. For example, Riesz et al. observed a COF in dry air of sapphire sliding against sapphire of 0.4–0.5 at room temperature.^[55] This is fully in line with our results for a COF of 0.45 reported for CuO–S. We speculate that the following processes take place (Figure S8, Supporting Information): (i) formation of wear particles, most likely comprised of a Cu–Al alloy and Al₂O₃ and (ii) oxidation of the wear particles surface (formation of CuO and Al₂O₃). The more wear particles

are generated, the more Al_2O_3 at the wear particles surface is in contact with the sphere and plate. These particles may then interact (a) adhesively with the sphere and (b) in a reducing fashion with the plate. Light microscopy of the sphere indicates that the wear particles are compacted at the sphere, continuously increasing the contact area (Figure S9, Supporting Information). Both processes, wear particle formation and growing contact area, may increase the COF successively. But why does this increased wear particle formation not occur for all experiments with CuO ? We speculate that the copper-rich patches formed for steady state COF experiments hinder the increased wear particle formation, due to an increased ductility.^[52] Such patches are not present on the sample with increased wear particle formation. What triggers this sudden increase in COF for the Cu_2O experiments and the onset of increased wear particle formation is still unclear. One hint is given in Figure S10, Supporting Information: Dark areas inside the wear track are observed, most likely being CuO formed while sliding. EDS measurements reveal an increased oxygen concentration of up to 40 at% in these regions (Table 4). Due to the acquisition settings (15 kV, 6.4 nA), some of the bulk Cu_2O may have contributed to these data of the CuO layer. The onset of CuO formation may trigger the sudden increase in COF. This may have two reasons: (i) the lower ductility of CuO in comparison with Cu_2O ^[52] and (ii) a change in wear mechanism. As discussed above, an adhesive wear mechanism occurs when CuO is present.

3.3. Influence of Oxide Formation on the Tribological Properties of Copper

The previous sections shed light on the tribological properties of copper oxides and discussed the resulting wear particles. Now we will try to answer the question if and how copper oxides induced through sliding alter the tribological performance of copper. Sliding on pure copper shows a coloring of the wear track together with a parallel decrease of the COF (Figures 3a, 4a, and 5). Such behavior is associated with simultaneous oxide formation (Figure 4a).^[1] A purplish color of the wear track is correlated with Cu_2O rather than CuO .^[1] EDS measurements after 10 000 cycles on Cu–OFHC reveal up to 22 ± 1 at% of oxygen inside the wear track (Table 3). Along with the presence of oxides (in the following called tribo-oxides), again yellowish wear particles are observed (up to 3 at% of aluminum, Table 3). The COF highlights the beneficial role of oxide formation during sliding (Figure 5): a friction reduction up to factor 1.4 (from ≈ 0.52 for 100–4000 cycles to ≈ 0.37 for 5000–10 000 cycles). Section 3.1 identified the different hardness, contact area, and shear strength as important factors influencing the coefficient of friction. Interestingly, the COF is still higher than the one for Cu_2O and CuO –S. Three major differences between the tribo-oxides and the pure oxides explain these results: (i) morphology, (ii) thickness, and (iii) surface coverage of the tribo-oxides. (i) The tribo-oxides' morphology–nanocrystalline Cu_2O areas in an amorphous matrix^[1]–deviates from that of the pure oxides. The semi-amorphous state of the oxides may further influence the COF.^[1] In amorphous Zr-based alloys, friction and wear were found to be slightly

lower in unlubricated conditions than for crystalline Ni alloys and steel.^[56] (ii) The thickness of the tribo-oxides is smaller than for all pure oxides (≈ 70 nm after 5000 cycles and 175 nm after 10 000 cycles, Figure S11, Supporting Information). For example, it is a factor 1000–2400 smaller than the thermally-oxidized Cu_2O thickness with ≈ 180 μm . (iii) The surface is not fully covered by the tribo-oxide.^[1] As a result of both, size and surface coverage, the contact conditions represent a mixture of copper and of the tribo-oxides. Collectively, the overall tribological behavior of the tribo-oxides hence differs from that of the pure oxides. Though the formed oxides are relatively small in comparison with the oxide layer thicknesses of up to ≈ 260 μm (Table 1), their capability of reducing the COF is almost beyond doubt. Even more, they hinder the sphere from indenting deeper into the material with high cycle numbers <5000 cycles. After 5000 cycles, the wear track mainly changes in width and not in depth (Figure 3b). The tribo-oxide thicknesses and widths increase concurrently (Figure S11, Supporting Information).

Considering our findings, tuning tribo-pairs in a way to generate an oxide layer can therefore be beneficial for many applications in order to improve friction and wear performance. This is of course only true if such an oxide formation is not detrimental for the respective contact and the stability of the oxide is guaranteed. For example, Quinn observed crack formation when tribo-oxide layers reach a critical thickness (usually 1 to 3 μm).^[57] Together with the increased wear particle formation, this demonstrates the twofold consequence of such oxide layers: Friction reduction on the one hand and increased wear particle formation on the other. Our findings underlie the need to fully understand the mechanisms determining the tribological performance of metal, or oxide tribo-pairs. In the case of oxidation, one might think about a controlled tribo-oxidation during the lifetime of the contact, or a deliberate pre-oxidation of the surface(s), for example, through a strategic heat treatment.

4. Conclusion

In summary, the effects of tribologically-induced oxide formation on the tribological performance of high-purity copper in a dry reciprocating sliding contact against sapphire have been systematically investigated. In addition, copper oxides (Cu_2O and CuO), representing the late stages of sliding on pure copper, were prepared, thoroughly characterized and tribologically loaded. Nano-indentation, Raman-, and X-ray spectroscopy were applied to characterize the oxides. The tribological properties as well as the wear track and particle morphologies were analyzed. Energy dispersive and X-ray photoelectron spectroscopy were used to examine the resulting wear particles.

Our findings allow to come to the following conclusions:

- Both oxides (Cu_2O and CuO) exhibit a lower COF than high-purity copper. This is mainly due to an increase in hardness and change in shear strength. The oxides therefore are a pivotal cause for the COF reduction during the tribological loading of high-purity copper. The hardness influence is stronger than the one from different surface roughnesses due to fabrication (sintering vs thermal oxidation) and preparation (electro-polishing vs untreated) methods.

- In the presence of copper oxides, irrespectively of whether they are formed during sliding or present from the beginning, reactions with the sapphire spheres are detected. As a result, copper and aluminum containing wear particles are observed. The majority of these wear particles do not alter the COF.
- A tribological-induced reduction of copper oxide during sliding against sapphire to metallic copper is found.
- Tribo-oxides on high-purity copper behave tribologically different than the respective pure oxides and exhibit a higher COF than the pure oxides for the same sliding distance. Considering their comparably small size and surface coverage with respect to the pure oxides, their potential for reducing the COF is enormous.

The broad implication of the present research is that tribo-oxidation for mild tribological loading can be beneficial for reducing friction. Our findings contribute to the fundamental understanding of tribo-oxidation in high-purity copper, especially in the late stages of sliding. Future research should consider the onset of increased wear particle formation more carefully, for instance, by investigating the influence of the counter body material.

5. Experimental Section

Materials: To compare bulk copper oxides with the tribologically-formed oxides during sliding, experiments with oxygen-free high conductivity (OFHC) copper, Cu₂O, and CuO were performed with a reciprocating linear tribometer.^[1,15,58,59] Cu–OFHC had a purity >99.95% (Goodfellow, Friedberg, Germany). Surfaces fully covered with Cu₂O and CuO were tested. For this purpose, Cu₂O and CuO layers were fabricated by thermal oxidation of electro-polished high-purity copper samples (air, T = 1000 °C, 1 h, quenched in water, muffle kiln, Nabetherm, Lilienthal, Germany). The results showed a two layer structure of the thermally oxidized samples: on-top of the Cu₂O layer, a CuO layer was formed. Additionally, a commercially available sintered CuO sample with a purity of 99.9% was purchased from Goodfellow (Bad Nauheim, Germany). Sapphire spheres with a diameter of 10 mm were used as counter bodies (Saphirwerk, Bruegg, Switzerland). The different samples were abbreviated as Cu–OFHC, Cu₂O, CuO–TO (thermally-oxidized), and CuO–S (sintered).

Oxide Characterization: Raman spectroscopy and X-ray diffraction were used to characterize the resulting oxides. Raman spectroscopy was performed with a Renishaw 1000 Raman micro spectrometer, using a Modu Aries-163 argon ion laser at 514.5 nm for excitation. The laser power was 1–2 mW at the sample spot of 1–2 μm in diameter using the x50 objective of the Leica-microscope. Spectra were taken in the spectral region between 150 and 1800 cm⁻¹. X-ray diffraction (XRD) was performed only on the grinded sample in ambient air with a Bruker D8 Advance diffractometer with an offset coupled theta/2theta scan type using Cu K-α radiation (λ = 1.5406 Å). Nano-indentation (Nanoindenter G200 XP, Agilent/Keysight Technologies, Inc., Santa Rosa, CA, United States) with a diamond Berkovich tip was performed to determine the oxides' hardness. After contacting the surface with the tip, the oxides were indented with a constant indentation strain rate (0.05 1/s) to a depth of 2 μm or 3 μm. The mechanical properties over the depth of indentation were determined by dynamic measurements employing the continuous stiffness measurement option of the instrument operated at a frequency of 45 Hz and an oscillation amplitude of 2 nm. The materials' properties were evaluated over suitable depth ranges (see Table 1). Ten indents with a spacing of 50 μm were performed. Surface roughness was measured with a confocal light microscope in interferometric mode

(Sensofar PLμ Neox, Barcelona, Spain). The oxide layer thickness was determined by micro sections. Cu–OFHC and Cu₂O grain sizes were evaluated with the linear intercept method.^[60]

Sample Preparation: Copper is known to readily oxidize at room temperature.^[61] To achieve a sample surface with no plastic deformation and minimal native oxidation from the environment, the high-purity copper samples were electro-polished right before the test. Details of the sample preparation are given in refs. [1,15]. By grinding the CuO layer on top of the thermally oxidized samples away, the Cu₂O samples were produced. Cu₂O and the CuO–S samples were prepared the same way as the high-purity copper samples. However, the electro-polishing step was replaced by a 15 min OPS-polishing to achieve a minimal surface roughness. The thermally-oxidized CuO sample was employed without additional preparation.

Experimental Setup: All experiments were performed with a stroke length of 12 mm in a reciprocating fashion for 5000 cycles in air at a relative humidity of 50% at room temperature without lubrication. One single experiment with high purity copper was performed with a stroke length of 12 mm for 10 000 cycles to investigate the oxidation at higher cycle numbers. Humidity and temperature during the tribological experiment were closely controlled. The normal load of 1.5 N was applied by a dead weight and the copper or copper oxide sample was moved by a linear motor (Precision Translation Stage, PI, Karlsruhe, Germany) with a sliding speed of 0.5 mm s⁻¹. The setup of the used reciprocating tribometer is described elsewhere.^[1,15,59]

Analysis Methods After Sliding: After the tribological testing, the surfaces were systematically analyzed. The plate and sphere were evaluated with a confocal light microscope, by investigating the depth and width of the wear track and a possible color change inside the wear track. Chemical changes inside the wear tracks were characterized by energy dispersive X-ray spectroscopy inside the scanning electron microscope (SEM) (FIB/SEM, FEI Helios 650, Hillsboro, Oregon USA; 15 kV, 6.4 nA). Cross-section electron microscopy images of the sintered CuO sample were prepared right after the tribological tests.^[62] The cross sections were cut out perpendicular to the sliding direction in the center of the wear track (see Supporting Information of ref. [1]). In order to protect the sample surface from ion beam damage when milling, two protective platinum layers (one with the electron and one with the ion beam) were deposited. Chemical composition depth profiles were recorded at the contact area of a sapphire sphere after 5000 sliding cycles against CuO–S. These measurements were performed with X-ray photoelectron spectroscopy XPS (PHI 5000 Versa Probe II, Ulvac-PHI, Inc. USA). The parameters for the spectra were 15 kV, 12.5 W, and the beam diameter was ≈50 μm.

Supporting Information

Supporting Information is available from the Wiley Online Library or from the author.

Acknowledgements

Partial funding of this work has been provided by the European Research Council under ERC Grant Agreement No. 771237, TriboKey. The authors thank P. Gruber and Y. Kang for the XRD measurements, and Eberhard Nold and Philipp Daum for the XPS measurements. The data that support the findings in this study are available from the link <https://doi.org/10.5445/IR/1000120846>.

Open access funding enabled and organized by Projekt DEAL.

Conflict of Interest

The authors declare no conflict of interest.

Keywords

copper, tribo-chemistry, tribology, X-ray photoelectron spectroscopy

Received: September 23, 2020

Revised: October 21, 2020

Published online:

- [1] Z. Liu, T. Höche, P. Gumbsch, C. Greiner, *Scr. Mater.* **2018**, 153, 114.
 [2] T. E. Fischer, H. Tomizawa, *Wear* **1985**, 105, 29.
 [3] M. Fink, *Trans. Amer. Soc. Steel Treat.* **1930**, 18, 1026.
 [4] W. G. Sawyer, N. Argibay, D. L. Burris, B. A. Krick, *Annu. Rev. Mater. Res.* **2014**, 44, 395.
 [5] R. A. Poggie, J. J. Wert, *Wear* **1992**, 156, 315.
 [6] Y. Zhang, J. Michael Shockley, P. Vo, R. R. Chromik, *Tribol. Lett.* **2016**, 62, 9.
 [7] H. So, D. S. Yu, C. Y. Chuang, *Wear* **2002**, 253, 1004.
 [8] T. S. Eyre, D. Maynard, *Wear* **1971**, 18, 301.
 [9] Y. Zhang, Y. Epshteyn, R. R. Chromik, *Tribol. Int.* **2018**, 123, 296.
 [10] T. F. J. Quinn, *Wear* **1971**, 18, 413.
 [11] A. Erdemir, G. Ramirez, O. L. Eryilmaz, B. Narayanan, Y. Liao, K. G., S. K. R. S. Sankaranarayanan, *Nature* **2016**, 536, 67.
 [12] H. Kato, K. Komai, *Wear* **2007**, 262, 36.
 [13] T. F. J. Quinn, *ASLE Trans.* **1967**, 10, 158.
 [14] D. Kuhlmann-Wilsdorf, *Wear* **1985**, 105, 187.
 [15] C. Greiner, Z. Liu, L. Strassberger, P. Gumbsch, *ACS Appl. Mater. Interfaces* **2016**, 8, 15809.
 [16] M. Carey-Lea, *Am. J. Sci.* **1893**, 46, 351.
 [17] F. H. Stott, G. C. Wood, *Tribol. Int.* **1978**, 11, 211.
 [18] M. F. Ashby, S. C. Lim, *Acta Metall.* **1987**, 35, 1.
 [19] J. L. Sullivan, T. F. J. Quinn, D. M. Rowson, *Tribol. Int.* **1980**, 13, 153.
 [20] J. Li, M. Elmadagli, V. Y. Gertsman, J. Lo, A. T. Alpas, *Mater. Sci. Eng., A* **2006**, 421, 317.
 [21] L. Pastewka, S. Moser, P. Gumbsch, M. Moseler, *Nat. Mater.* **2011**, 10, 34.
 [22] X. Chen, Z. Han, K. Lu, *Scr. Mater.* **2015**, 101, 76.
 [23] F. H. Stott, J. Glascott, G. C. Wood, *Wear* **1985**, 101, 311.
 [24] H. Hong, R. F. Hochman, T. F. J. Quinn, *Tribol. Trans.* **1988**, 31, 71.
 [25] J. F. Archard, W. Hirst, *Proc. R Soc. London* **1956**, A236, 394.
 [26] J. E. Wilson, F. H. Stott, G. C. Wood, *Proc. R. Soc. London, Ser. A* **1980**, 369, 557.
 [27] I. A. Inman, P. K. Datta, H. L. Du, J. S. Burnell-gray, S. Pierzgaliski, Q. Luo, *Tribol. Int.* **2005**, 38, 812.
 [28] J. Jiang, F. H. Stott, M. M. Stack, *Tribol. Int.* **1998**, 31, 245.
 [29] F. F. Tao, *ASLE Trans.* **1969**, 12, 97.
 [30] C. Gattinoni, A. Michaelides, *Surf. Sci. Rep.* **2015**, 70, 424.
 [31] L. De Los Santos Valladares, D. H. Salinas, A. B. Dominguez, D. A. Najarro, S. I. Khondaker, T. Mitrelias, C. H. W. Barnes, J. A. Aguiar, Y. Majima, *Thin Solid Films* **2012**, 520, 6368.
 [32] S.-K. Lee, H.-C. Hsu, W.-H. Tuan, *Mater. Res.* **2016**, 19, 51.
 [33] P. J. Blau, *J. Tribol.* **1985**, 107, 483.
 [34] M. Sedlaček, B. Podgornik, J. Vižintin, *Wear* **2009**, 266, 482.
 [35] K. J. Kubiak, T. W. Liskiewicz, T. G. Mathia, *Tribol. Int.* **2011**, 44, 1427.
 [36] G. Zhou, J. C. Yang, *Surf. Sci.* **2003**, 531, 359.
 [37] K. Heinemann, D. B. Rao, D. L. Douglass, *Oxid. Met.* **1975**, 9, 379.
 [38] A. J. W. Moore, W. J. M. Tegart, *Proc. R. Soc. A* **1952**, 212, 452.
 [39] D. Kümmel, M. Hamann-Schroer, H. Hetzner, J. Schneider, *Wear* **2019**, 422–423, 261.
 [40] T. Oishi, M. Goto, A. Kasahara, M. Tosa, *Surf. Interface Anal.* **2004**, 36, 1259.
 [41] S. Meghana, P. Kabra, S. Chakraborty, N. Padmavathy, *RSC Adv.* **2015**, 5, 12293.
 [42] Y. Deng, A. D. Handoko, Y. Du, S. Xi, B. S. Yeo, *ACS Catal.* **2016**, 6, 2473.
 [43] J. Han, X. Zong, X. Zhou, C. Li, *RSC Adv.* **2015**, 5, 10790.
 [44] A. Singhal, M. R. Pai, R. Rao, K. T. Pillai, I. Lieberwirth, A. K. Tyagi, *Eur. J. Inorg. Chem.* **2013**, 2013, 2640.
 [45] Y. Zhu, K. Mimura, J. W. Lim, M. Isshiki, Q. Jiang, *Metall. Mater. Trans. A* **2006**, 37, 1231.
 [46] F. P. Bowden, D. Tabor, *The Friction and Lubrication of Solids*, Oxford University Press, New York **1950**.
 [47] T. Mishra, M. de Rooij, M. Shisode, J. Hazrati, D. J. Schipper, *Wear* **2019**, 436–437, 203042.
 [48] D. H. Buckley, *Surface Effects in Adhesion, Friction, Wear, and Lubrication*, Elsevier Scientific Publishing Company, Amsterdam **1981**.
 [49] T. Kayaba, K. Kato, *ASLE Trans.* **1981**, 24, 164.
 [50] B. J. Babalola, M. O. Bodunrin, J. O. Borode, K. K. Alaneme, *J. Miner. Mater. Charact. Eng.* **2013**, 1, 245.
 [51] M. A. Shaik, B. R. Golla, *Tribol. Int.* **2019**, 136, 127.
 [52] K. Dies, *Kupfer Und Kupferlegierungen in Der Technik*, Springer, Berlin **1967**.
 [53] R. A. Poggie, J. J. Wert, L. A. Harris, R. A. Poggie, J. J. Wert, L. A. Harris, *J. Adhes. Sci. Technol.* **1994**, 8, 11.
 [54] Y. Li, T. L. Ngai, W. Xia, *Wear* **1996**, 197, 130.
 [55] C. H. Riesz, H. S. Weber, *Wear* **1964**, 7, 67.
 [56] P. J. Blau, *Wear* **2001**, 250, 431.
 [57] T. F. J. Quinn, *Tribol. Int.* **1983**, 16, 257.
 [58] C. Greiner, M. Schäfer, U. Popp, P. Gumbsch, *ACS Appl. Mater. Interfaces* **2014**, 6, 7986.
 [59] X. Chen, R. Schneider, P. Gumbsch, C. Greiner, *Acta Mater.* **2018**, 161, 138.
 [60] Advanced Technical Ceramics – Monolithic Ceramics; General and Textural Properties – Part 3: Determination of Grain Size and Size Distribution (Characterized by the Linear Intercept Method); German Version EN 623-3:2001, **2003**.
 [61] I. Platzman, R. Brener, H. Haick, R. Tannenbaum, *J. Phys. Chem. C* **2008**, 112, 1101.
 [62] C. A. Volkert, A. M. Minor, *MRS Bull.* **2007**, 32, 389.